Computation of Propagation Characteristics of Chiral Layered Waveguides

Gonzalo Plaza, Francisco Mesa, and Manuel Horno, *Member, IEEE*

***Abstract*—In this paper the authors present a systematic numerical method to analyze multilayered linear chiral waveguides. The Maxwell's equations are solved inside each layer and the transversal fields at the top and bottom of the whole layered medium are then related. This relation, together with the use of the proper transversal impedance matrices, makes it possible to obtain the dispersion relation of the waveguide. Since this technique is mainly numerical, the whole procedure is practically independent of both the number of layer and linear properties of the materials. In addition to the proper modes, the authors also show the behavior of the improper leaky modes of different chiral waveguides. In all the analyzed cases and for the considered ranges, the authors have found that the presence of chiral material does not substantially change the qualitative behavior of the dispersion relation, although it offers another parameter to control the propagation characteristics of the waveguide.**

***Index Terms*—Chiral, spectral domain, planar wageguide.**

I. Introduction

IN THE PAST few years, the attention paid to the study of electromagnetic propagation in biisotropic and bianisotropic chiral media has increased notably. This increasing interest is raised by the potential applications of the chiral material as well as its theoretical and academic significance. As is well known, a chiral object is one that cannot be brought into congruence with its mirror image by translation or rotation [1]. A collection of such objects is then characterized by right or left handedness and, therefore, chirality means a lack of bilateral symmetry. The most outstanding properties of chiral media concerning the propagation of electromagnetic fields are reported to be their ability either for rotating the plane of polarization of an electromagnetic wave or for circular dichroism [2]. Although today there are no known natural media showing chiral properties at microwave and millimeter frequencies, the progress in the polymers science is expected to make these media of common use in future technology (currently, these media are manufactured by embedding polymers with chiral structure into a host dielectric media) [1], [3]. In this event, many of the proposed devices whose performance lies on the chiral properties of the media could be built. A general survey of chiral devices is reported in [3].

The electromagnetic propagation in chiral materials has been extensively studied in the literature. General features on the bi(iso/ani)sotropic materials are presented in [4], [5] and different aspects about electromagnetic propagation in homogeneous unbounded bi(iso/ani)sotropic media are considered in [6]–[11]. Propagation along closed waveguides homogeneously filled with biisotropic materials has been considered for example in [12], [13]–[14]; parallel-plate waveguides homogeneously filled with biisotropic material are treated in [15] and inhomogeneously filled with these media in [16], [17]; open chiroslab waveguides are studied in [18], [19]. In [20]–[22] waveguides with isotropic chiral materials and gyrotropic properties (chiroferrites and chiroplasmas) are considered. A microstrip on a biisotropic substrate is analyzed in [23].

In this paper, the authors propose a systematic quasi-numerical method to analyze general laterally open waveguides with layered media whose layers can exhibit linear bianisotropic properties without restriction. One of the main features of the method presented here is that the increasing of the number of layers, as well as its complexity, hardly affects its efficiency. Here, the technique of analysis used follows the guidelines presented in [24], although the present work is now specifically focussed on the analysis of general layered chiral waveguides, including some novel structures combining gyrotropic and chiral anisotropic properties. The propagation characteristics of the different structures are computed following a 4×4 transition matrix scheme to solve the Maxwell's equations inside the bianisotropic layers. This scheme has been used often in the past [24]–[27] as it has been shown to be very suitable in dealing with general anisotropic materials.

Finally, the authors present the propagation characteristics of some types of chiral waveguides. Specifically, the authors have analyzed the behavior of the propagation constants when some characteristic parameters are varied. The authors' study has shown that the influence of the chirality parameters on the waveguide characteristics in the analyzed range is similar to that provided by the usual varying of the dielectric permittivity or magnetic permeability. This study is extended to both the proper and improper modes of the chiral waveguides.

II. Analysis

In this section, the authors present the theoretical treatment to analyze the planar multilayered waveguide shown in Fig. 1. Since the authors' aim is to develop as general an analysis as possible, each substrate in the above structure is assumed to show linear bianisotropic electromagnetic properties, and the top and bottom waveguide interfaces can be any of those susceptible to being implemented by impedance matrices

Manuscript received June 7, 1996; revised December 24, 1996. This work was supported by the DGICYT, Spain, Project TIC95-0447.

The authors are with the Department of Electronics and Electromagnetism, Microwave Group, University of Seville, 41012 Seville, Spain.

Publisher Item Identifier S 0018-9480(97)02535-0.

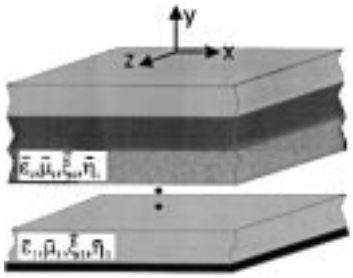

Fig. 1. Multilayered waveguide including general bianisotropic materials.

(i.e., electric/magnetic walls, vacuum medium, periodically loaded interfaces, ...). One of the possible ways of writing the constitutive relations for the most general bianisotropic medium is given in [27], [28]:

$$\mathbf{D} = \epsilon_0 \bar{\epsilon}_r \cdot \mathbf{E} + \frac{1}{c}\,\bar{\xi}_r \cdot \mathbf{H} \tag{1}$$

$$\mathbf{B} = \mu_0 \bar{\mu}_r \cdot \mathbf{H} + \frac{1}{c}\,\bar{\eta}_r \cdot \mathbf{E} \tag{2}$$

where $c = 1/\sqrt{\epsilon_0 \mu_0}$, $\bar{\epsilon}_r$ and $\bar{\mu}_r$ are the relative dyadic permittivity and permeability, and $\bar{\xi}_r$ and $\bar{\eta}_r$ are the cross-coupling dyads accounting for the chirality of the substrate (note that these four dyads are dimensionless and that care must be taken concerning the physical meaning of $\bar{\epsilon}_r$ [4], [29]).

The following time and spatial harmonic dependence are assumed for the electromagnetic fields

$$\mathbf{A}(\mathbf{r}, t) = \mathbf{A}(y) e^{-j(k_x x + k_z z)} e^{j\omega t} \tag{3}$$

although, the explicit time dependence $e^{j\omega t}$ will be suppressed throughout.

Using the constitutive relations (1)–(2), the Maxwell's equations for the curls inside each layer are

$$\nabla \times \mathbf{E} = -j\omega \left(\mu_0 \bar{\mu}_r \cdot \mathbf{H} + \frac{1}{c}\,\bar{\eta}_r \cdot \mathbf{E} \right) \tag{4}$$

$$\nabla \times \mathbf{H} = j\omega \left(\epsilon_0 \bar{\epsilon}_r \cdot \mathbf{E} + \frac{1}{c}\,\bar{\xi}_r \cdot \mathbf{H} \right). \tag{5}$$

In view of the spatial dependence shown in (3), the $\nabla\times$ operator can be expressed in matricial form as

$$\nabla\times \equiv \begin{bmatrix} 0 & jk_z & \frac{\partial}{\partial y} \\ -jk_z & 0 & jk_x \\ -\frac{\partial}{\partial y} & -jk_x & 0 \end{bmatrix}. \tag{6}$$

Using this operator, the second and fifth row equations in the set (4)–(5) can be written as

$$-jk_z E_x + jk_x E_z = -j\omega(\bar{\mu}_y \cdot \mathbf{H} + \bar{\eta}_y \cdot \mathbf{E}) \tag{7}$$

$$-jk_z H_x + jk_x H_z = j\omega(\bar{\epsilon}_y \cdot \mathbf{E} + \bar{\xi}_y \cdot \mathbf{H}) \tag{8}$$

where $\bar{\mu}_y$ and $\bar{\eta}_y$ are defined as follows:

$$\bar{\mu}_y = \mathbf{a}_y \cdot \bar{\mu} = \mu_0(\mu_{yx}\mathbf{a}_x + \mu_{yy}\mathbf{a}_y + \mu_{yz}\mathbf{a}_z)$$

$$\bar{\eta}_y = \mathbf{a}_y \cdot \bar{\eta} = \frac{1}{c}(\eta_{yx}\mathbf{a}_x + \eta_{yy}\mathbf{a}_y + \eta_{yz}\mathbf{a}_z)$$

where $\mathbf{a}_x$, $\mathbf{a}_y$, and $\mathbf{a}_z$ stand for the unit vectors along the cartesian axes. Similar expressions hold for $\bar{\epsilon}_y$ and $\bar{\xi}_y$.

Since expressions (7) and (8) are algebraic, both E_y and H_y can be expressed in terms of the remaining components of the fields in the following way:

$$H_y = \bar{Y} \cdot \mathbf{E}_t + \bar{W} \cdot \mathbf{H}_t \tag{9}$$

$$E_y = -\bar{Y}^D \cdot \mathbf{H}_t + \bar{W}^D \cdot \mathbf{E}_t \tag{10}$$

where $\mathbf{E}_t = E_x\mathbf{a}_x + E_z\mathbf{a}_z, \mathbf{H}_t = H_x\mathbf{a}_x + H_z\mathbf{a}_z$ (subscript t means transversal to y-direction), and $\bar{Y}$ and $\bar{W}$ are given by

$$\bar{Y} = \frac{\epsilon_{yy}(\bar{u} + \bar{\eta}_{yt}) - \eta_{yy}\bar{\epsilon}_{yt}}{\eta_{yy}\xi_{yy} - \mu_{yy}\epsilon_{yy}} \tag{11}$$

$$\bar{W} = \frac{\eta_{yy}(\bar{u} - \bar{\xi}_{yt}) + \epsilon_{yy}\bar{\mu}_{yt}}{\eta_{yy}\xi_{yy} - \mu_{yy}\epsilon_{yy}} \tag{12}$$

with $\bar{u} = -k_z/\omega\mathbf{a}_x + k_x/\omega\mathbf{a}_z$ and $\bar{\eta}_{yt} = \eta_{yx}\mathbf{a}_x + \eta_{yz}\mathbf{a}_z$. Similar expressions hold for $\bar{\epsilon}_{yt}$, $\bar{\xi}_{yt}$, and $\bar{\mu}_{yt}$. $\bar{Y}^D$ and $\bar{W}^D$ stand for the dual of the $\bar{Y}$ and $\bar{W}$, respectively; that is, their expressions can be obtained directly from (11) and (12) using the dual relations [6]

$$\begin{aligned} \bar{\mu} &\leftrightarrow \bar{\epsilon} \\ \bar{\xi} &\leftrightarrow -\bar{\eta}. \end{aligned} \tag{13}$$

Substituting (9) and (10) into the remaining row of Maxwell's equations in (4)–(5), the following matrix differential equation is obtained for the transversal fields:

$$\frac{\partial}{\partial y}\begin{bmatrix} E_x \\ E_z \\ H_x \\ H_z \end{bmatrix} = j\omega \begin{bmatrix} \bar{A}_1 & \bar{B}_1 \\ \bar{A}_2 & \bar{B}_2 \\ -\bar{B}_1^D & \bar{A}_1^D \\ -\bar{B}_2^D & \bar{A}_2^D \end{bmatrix} \cdot \begin{bmatrix} \mathbf{E}_t \\ \mathbf{H}_t \end{bmatrix} = j\omega[\mathbf{Q}] \cdot \begin{bmatrix} E_x \\ E_z \\ H_x \\ H_z \end{bmatrix} \tag{14}$$

where

$$\bar{A}_1 = \bar{\eta}_{zt} - \left(\frac{k_x}{\omega} - \eta_{zy} \right) \bar{W}^D + \mu_{zy}\bar{Y} \tag{15}$$

$$\bar{A}_2 = -\bar{\eta}_{xt} - \left(\frac{k_z}{\omega} + \eta_{xy} \right) \bar{W}^D - \mu_{xy}\bar{Y} \tag{16}$$

$$\bar{B}_1 = \left(\frac{k_x}{\omega} - \eta_{zy} \right) \bar{Y}^D + \bar{\mu}_{zt} + \mu_{zy}\bar{W} \tag{17}$$

$$\bar{B}_2 = \left(\frac{k_z}{\omega} + \eta_{xy} \right) \bar{Y}^D - \bar{\mu}_{xt} - \mu_{xy}\bar{W}. \tag{18}$$

Note that $[\mathbf{Q}]$ is a 4×4 matrix. The corresponding dual expressions for $\bar{A}$ and $\bar{B}$ arrays, denoted with superscript D, can be obtained from (15)–(18) by means of (13) and the additional dual relations

$$\begin{aligned} \bar{Y} &\leftrightarrow \bar{Y}^D \\ \bar{W} &\leftrightarrow \bar{W}^D. \end{aligned} \tag{19}$$

After solving the matrix differential equation (14), the transversal fields at the top of the ith layer can be written as a function of the transversal fields at the bottom of this layer:

$$\begin{bmatrix} \mathbf{E}_t \\ \mathbf{H}_t \end{bmatrix}_{T,i} = [\mathbf{P}]_i \cdot \begin{bmatrix} \mathbf{E}_t \\ \mathbf{H}_t \end{bmatrix}_{B,i} \tag{20}$$

where subscripts B and T indicate bottom and top, respectively, and the $[\mathbf{P}]_i$ matrix is given by

$$[\mathbf{P}]_i = \exp(j\omega[\mathbf{Q}]_i h_i) \tag{21}$$

with h_i being the height of the layer [24]. A similar study for computing the transition matrix $[\mathbf{P}]_i$, but in a different context, is presented in [27].

In order to find the dispersion equation for the waveguide, and considering that the transversal fields must be continuous at the interfaces, (20) is applied repeatedly starting from the bottom layer of the multilayered structure up to the upper layer. Although the following mathematical steps were partially exposed in [24], the authors will detail some of them for the sake of completeness. In this way, the top transversal field of the guide can be related to the bottom transversal field as follows:

$$\begin{bmatrix}\mathbf{E}_t\\ \mathbf{H}_t\end{bmatrix}_T = [\mathbf{P}]\cdot\begin{bmatrix}\mathbf{E}_t\\ \mathbf{H}_t\end{bmatrix}_B \tag{22}$$

where subscripts B and T now means bottom and top of the whole multilayered structure, and

$$[\mathbf{P}] = \Pi_{i=1}^{i=N}[\mathbf{P}]_i \tag{23}$$

with N being the total number of layers in the structure (note that $[\mathbf{P}]$ is a 4×4 matrix). Equation (22) stands for an homogeneous linear system of four equations with eight unknowns, namely, the transversal components of the electromagnetic fields at the top and bottom of the guide . The authors can add the four remaining equations including the relation between the electric and magnetic transversal fields given by the 2×2 impedance matrix $[\mathbf{Z}]$

$$\mathbf{E}_t = [\mathbf{Z}]\cdot\mathbf{H}_t. \tag{24}$$

This equation holds for both the bottom and top transversal fields of the structure, so four more equations are available together with the four previous ones presented in (22). In this work, the authors will consider only two possible situations for the impedance matrix: a perfect electric wall and a boundary with vacuum. In the first case, the impedance matrix is the null matrix, while in the second one, the vacuum impedance matrix (considering the spatial dependence of the fields in (3)) can be easily obtained from the Maxwell's equations

$$\begin{bmatrix}E_x\\ E_z\end{bmatrix} = \frac{1}{\omega\epsilon_0 k_y}\begin{bmatrix}-k_x k_z & -k_0^2+k_x^2\\ k_0^2-k_z^2 & k_x k_z\end{bmatrix}\begin{bmatrix}H_x\\ H_z\end{bmatrix} \tag{25}$$

where k_0 is the vacuum wavenumber and $k_y = \sqrt{k_0^2-k_x^2-k_z^2}$. It should be noted that the sign of the imaginary part of k_y determines the proper/improper nature of the modes [29].

Combining (22) and the impedance relations, the following linear homogeneous system can be obtained:

$$\begin{bmatrix}[\mathbf{P}]_{11}[\mathbf{Z}]_B+[\mathbf{P}]_{12} & -[\mathbf{Z}]_T\\ [\mathbf{P}]_{21}[\mathbf{Z}]_B+[\mathbf{P}]_{22} & -[\mathbf{I}]\end{bmatrix}\begin{bmatrix}\mathbf{H}_{t,B}\\ \mathbf{H}_{t,T}\end{bmatrix} = \begin{bmatrix}\mathbf{0}\\ \mathbf{0}\end{bmatrix} \tag{26}$$

where $[\mathbf{P}]_{i,j}$ stands for any of the 2×2 boxes of the 4×4 matrix $[\mathbf{P}]$, $[\mathbf{I}]$ is the 2×2 unit matrix, and $\mathbf{0}$ is the two-components null vector. Equivalently, the authors can express the 4×4 eigensystem (26) as

$$\{[\mathbf{P}]_{1,1}[\mathbf{Z}]_B+[\mathbf{P}]_{1,2}-[\mathbf{Z}]_T([\mathbf{P}]_{2,1}[\mathbf{Z}]_B+[\mathbf{P}]_{2,2})\}\cdot\mathbf{H}_{t,B} = \mathbf{0}. \tag{27}$$

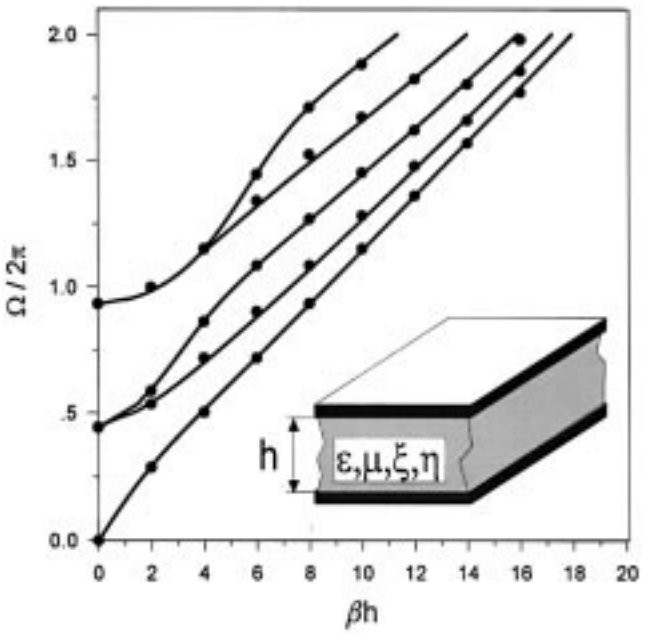

Fig. 2. Brillouin diagram for propagating modes in an homogeneous bi-isotropic lossless and reciprocal closed waveguide. β stands for the phase constant, $\Omega = \omega h\sqrt{\mu\epsilon}$, $\epsilon_r = 1.142\,12$, $\mu_r = 1$, $\xi_r = -j\,0.376\,99$, and $\eta = -\xi$. The authors' results: (——); results in [15]: (•).

Forcing the above homogeneous system to have solutions provides the dispersion relation of the guide

$$\det[\mathbf{M}(k_x, k_z, \omega)] = 0 \tag{28}$$

with $[\mathbf{M}]$ being the 2×2 coefficient matrix of (27).

In practice, and since there is not always cylindrical symmetry, the authors have assumed a propagation direction along the z-axis and, therefore, a propagation constant $k_z = \beta_z + j\alpha_z$. Any fixed external direction (for example, the biasing direction) is then referred to the propagation direction after imposing $k_x = 0$. The searching for the zeros of (28) can be efficiently performed by means of any of the usual differential or integral methods because the function $\det[\mathbf{M}(k_x, k_z, \omega)]$ does not have any pole [24].

Since the authors' aim has been to deal with very general structures, they could not develop the usual analytical treatment found in previous works dealing with specific structures. Thus, the authors have presented a systematic numerical scheme to compute the dispersion relation of the planar waveguides. However, despite this lack of analytical details, the authors can readily identify the main features of the fields by numerically computing them. For this purpose, the authors can compute the eigenvector $\mathbf{H}_{t,B}$ of (27) and then obtain the $\mathbf{E}_{t,B}$ vector via the impedance matrix $[\mathbf{Z}]_B$. Once these vectors are computed, the transversal components of the fields at any interface are calculated using the transition matrices $[\mathbf{P}]_i$. The y-components of the fields can also be readily computed via (9) and (10).

III. Numerical Examples

Following the scheme showed in the previous section, the authors have developed a computer code to compute the

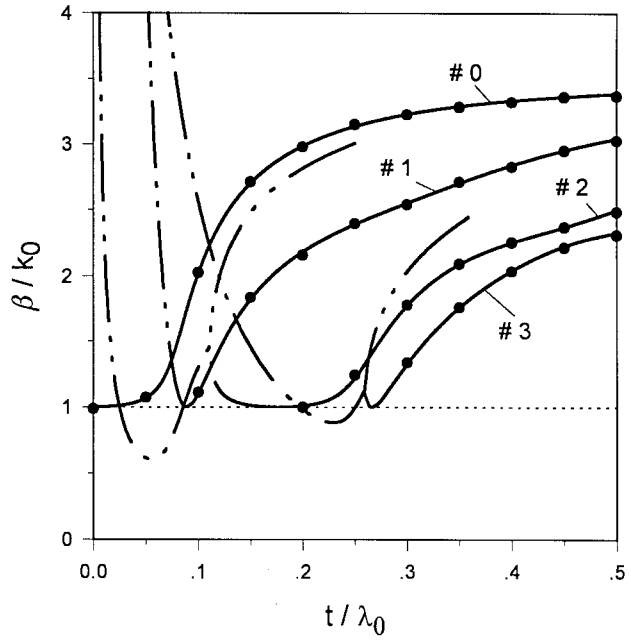

(a)

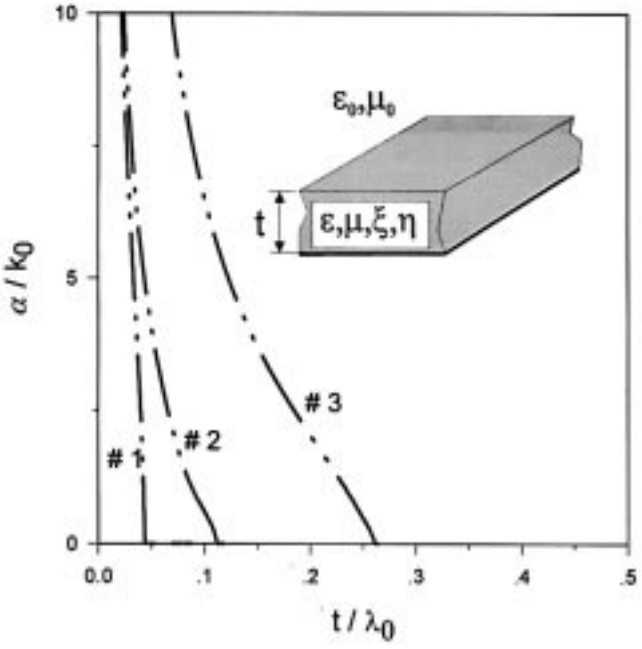

(b)

Fig. 3. Dispersion diagram for (a) the normalized phase constant β/k_0, and (b) for the normalized attenuation constant α/k_0, corresponding to the proper and improper modes in the biisotropic lossless reciprocal open waveguide shown in Fig. 3(b). The authors' results: (———) proper modes, (– – · · – –) improper modes; data in [18]: (•). Relative permittivity $\varepsilon_r = 9$, relative permeability $\mu_r = 1$, chirality parameters $\xi_r = \eta_r^* = -j0.5$; λ_0 stands for the vacuum wavelength, k_0 stands for the vacuum wavenumber.

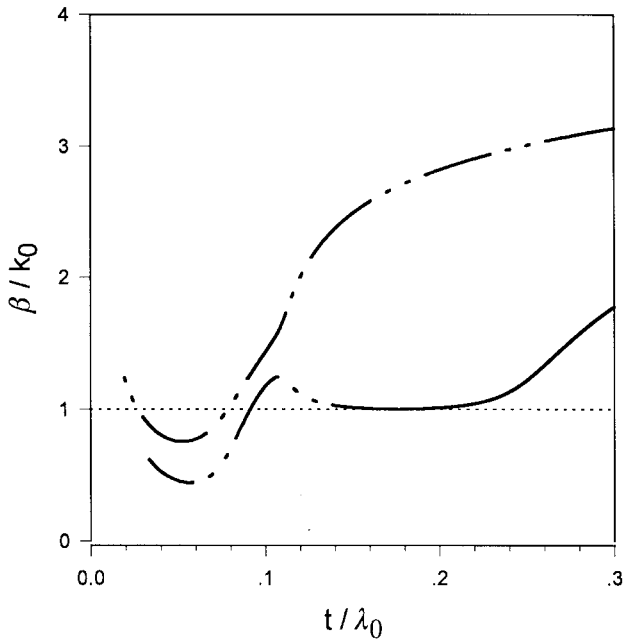

(a)

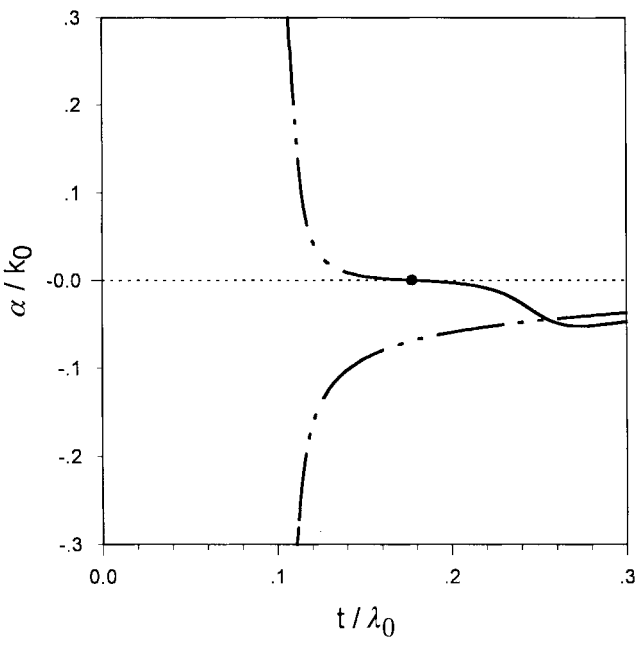

(b)

Fig. 4. Dispersion diagram for (a) the normalized phase constants and (b) the normalized attenuation constants of the proper mode # 2 and its corresponding improper mode. The waveguide is shown in Fig. 3(b), but assuming now a conductivity $\sigma = 0.0001$ S/mm: (———) proper mode, (– – · · – –) improper mode.

dispersion relation and fields of the aforementioned general planar waveguides. The authors have carefully checked their results with previous data reported by other authors.

First, the authors analyze a parallel-plate chirowaveguide filled with an homogeneous biisotropic reciprocal and lossless medium. The results of the authors' analysis, together with those reported in [15], are plotted in Fig. 2, showing an excellent agreement. It is interesting to note that as in [15], the authors have also found a mode of zero cutoff frequency (namely, the dominant mode of the chirowaveguide) and an small region of modal degeneracy at the onset of higher modes. All the modes of this chiral structure (including the dominant one) are hybrid [12], although as the chirality admittance goes to zero the dominant mode turns into a TEM mode and the remaining modes become E-modes or H-modes.

As a second example, Fig. 3(a) and (b) show the authors' analysis of the same grounded chiroslabguide previously stud-

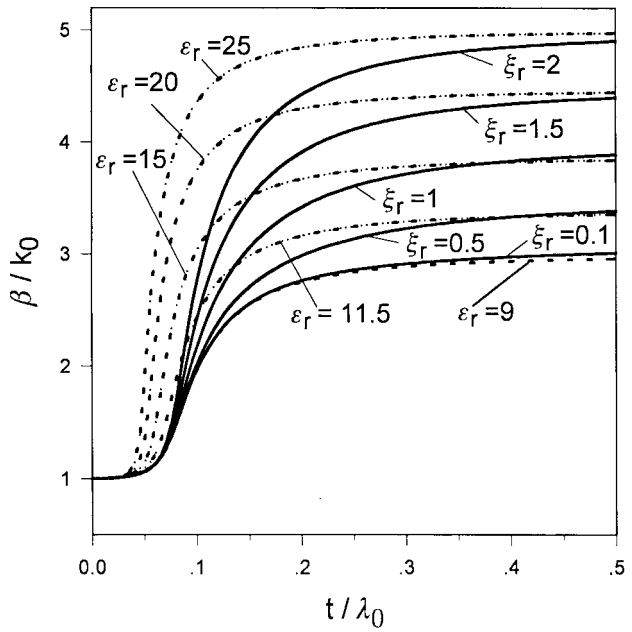

Fig. 5. Normalized phase constant for the fundamental mode of the waveguide shown in Fig. 3(b) for different values of the permittivity and the parameter of chirality. Chiral case: (——), nonchiral case ($\cdots$). In the chiral case $\epsilon_r = 9$ for all the different values of $\xi_r = \eta_r^*$. In this figure, ξ_r is a negative, imaginary quantity.

ied in [18] (the waveguide is shown in Fig. 3(b)). As for the dispersion relation of the surface modes, the authors have found an excellent agreement with the data of Fig. 3(a) in [18], but in addition, the authors have plotted the propagation constants for some improper real and complex modes. It can be seen in Fig. 3(a) and (b) that each higher-surface mode becomes a real improper mode at a certain frequency, often denoted as the cutoff frequency. As usual, in nonchiral open guides [24], [30], as the frequency decreases this improper real mode joins together with another improper real mode to yield a pair of complex conjugate improper modes (the so-called *leaky* modes).

The authors have also studied the behavior of the quasi-modes when conductivity losses are assumed in the substrate ($\sigma = 0.0001$ S/mm). For clarity, the authors only consider the behavior of a pair of modes: the second quasi-mode and its corresponding improper mode. The behavior of the normalized phase and attenuation constants for this case are shown in Fig. 4(a) and (b), respectively. It can be seen in Fig. 4(a) that as frequency decreases, the proper complex mode (that is, the perturbed surface mode due to the substrate losses) turns into an improper complex mode at $\beta/k_0 = 1$. At this very point, the attenuation constant (see Fig. 4(b)), which was negative, gets null to later take large positive values as frequency keeps on decreasing. The corresponding improper mode presents negative values of the attenuation constant for all of the ranges of frequencies shown in Fig. 4(b). Note that the behavior of the phase constants of both the proper and improper modes is similar to that corresponding to the lossless case, but now the presence of losses preclude the modes from joining together to form a pair of improper complex conjugate modes as in

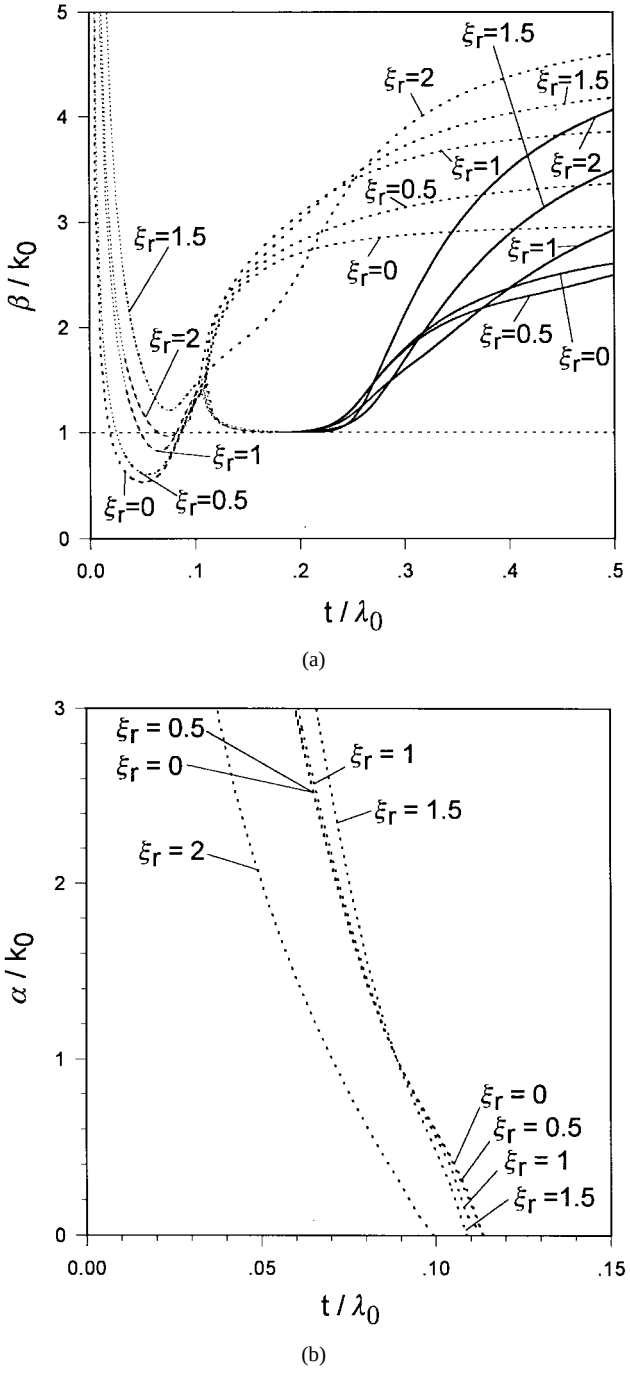

Fig. 6. Dispersion diagram for (a) the normalized phase constant and (b) the normalized attenuation constant of the second higher mode of the waveguide shown in Fig. 3(b) for different values of the chirality parameter. $\epsilon_r = 9$ and $\mu_r = 1$ for all the different values of $\xi_r = \eta_r^*$: (——) proper modes, ($\cdots$) improper modes.

the lossless case. It should be noted that this latter effect also appears in nonchiral waveguides.

Next, and similar to [18], the authors have studied the behavior of the fundamental surface mode of the lossless grounded chiroslab as a function of the chirality in Fig. 5. The curves of this figure show that the chirality significantly affects the phase constant of this mode (specifically, the higher the chirality, the slower the wave). The chirality parameter could then be used as another variable to control the modal

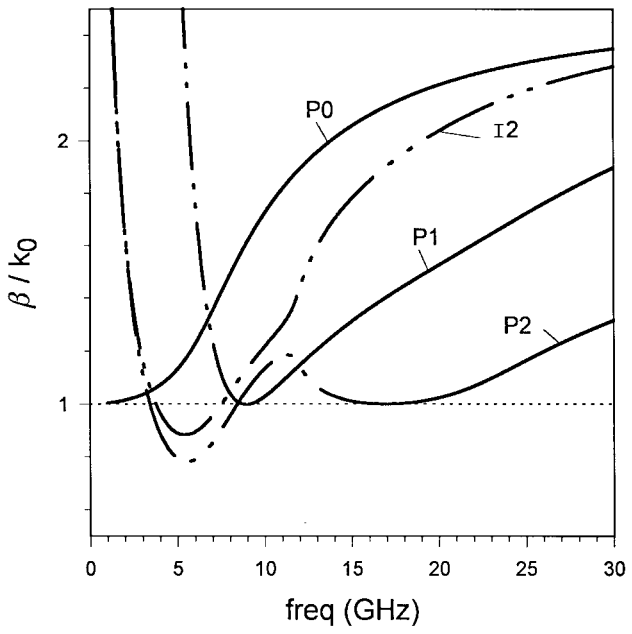

(a)

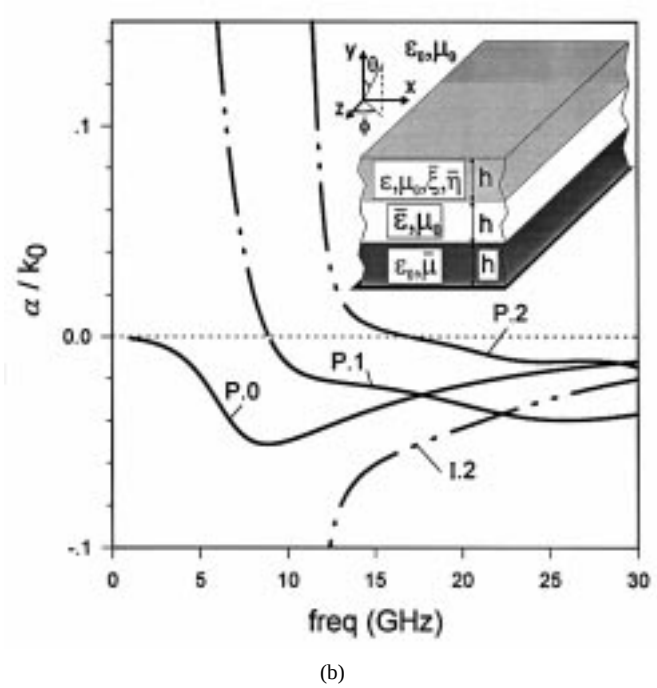

(b)

Fig. 7. Dispersion diagram for (a) the normalized phase constants and (b) the normalized attenuation constants of the proper and improper modes propagating along the positive z-direction in the three-layered bianisotropic nonreciprocal waveguide shown in Fig. 7(b). Dimensions: $h = 5$ mm. Lossless fully-saturated ferrite: $H_0 = 900$ Oe, $4\pi M_s = 750$ G, $\epsilon_r = 1$; Plasma: $H_0 = 900$ Oe, $\epsilon_r = 1$, $n = 10^{15}$ m^{-3}, $\tau = 10^{-12}$ s, $m^* = 0.06678 m_e$, $\mu_r = 1$; Biasing magnetic-field direction: $\theta = 45^0$, $\phi = 45^0$; Lossless bianisotropic layer: $\epsilon_r = 4, \mu_r = 1, \xi_{r,xx} = 0.1 - j0.5$, $\xi_{yy} = \xi_{xx}$, $\xi_{r,zz} = -0.2 - j0.3$, $\xi_{ij} = 0 \ \ (i \neq j)$, $\bar{\eta} = \bar{\xi}^{\dagger}$ ($\bar{\xi}^{\dagger}$ stands for the transposed and conjugated of $\bar{\xi}$).

phase velocity of these structures. The authors have also plotted in Fig. 5 the behavior of the fundamental mode for different values of the dielectric permittivity, but assuming now $\xi = \eta = 0$ (nonchiral case). As can be seen in Fig. 5, it is possible to obtain similar phase velocities by either increasing the chirality or using high dielectric permittivity media. For example, similar values of the phase velocity are obtained using $\epsilon_r = 20$ in a nonchiral waveguide or using $\epsilon_r = 9$ and $\xi_r = -j1.5$ in the chiral waveguide. Thus, regarding the fundamental mode, the use of chiral materials could be an alternative to the use of high permittivity substrates.

In completing the above study, the authors have also considered the effect of the increase of the chirality parameters on the higher modes in Fig. 6(a) and (b). Fig. 6(a) shows the behavior of the normalized phase constant of the second higher proper mode (mode #2 in Fig. 3(a)) and its corresponding improper mode for different values of the chiral parameter ξ, including the nonchiral case. As can be seen in this figure, the increasing of the chirality in the considered range does not provide a qualitative behavior essentially different from that corresponding to the nonchiral case. Thus, as in the nonchiral case, the proper real mode becomes an improper real mode at $\beta/k_0 = 1$ to later meet its corresponding improper mode, thus yielding a leaky mode. It is also interesting to note that the cutoff frequency does not seem to be affected by the increasing of the chirality. The behavior of the attenuation constant is plotted in Fig. 6(b), showing newly similar features to those of the nonchiral case.

Finally, the authors present an example of a complex multilayered waveguide in order to show the possibilities of the present method for studying the potential applications of any kind of chiral composite materials. Specifically, the authors have chosen a grounded waveguide composed of three layers with different electric and magnetic properties (see Fig. 7(b)). The bottom layer is a fully saturated ferrite externally biased by a magnetic field; the second layer is a semi-conductor biased by the above-mentioned magnetic field and the top layer is an anisotropic lossless nonreciprocal chiral material. In Fig. 7(a) and (b), the authors have plotted the dispersion diagram for the phase and attenuation constants respectively assuming a forward propagation $(+z)$; a similar dispersion diagram is found, but not shown, for backward propagation. The authors have considered both proper and improper modes ranging from 0 to 30 GHz. As can be seen in these Fig. 7(a) and (b), the behavior of the phase and attenuation constants for the different modes are similar to that shown in the previous examples. Similar to the second example in the lossy case, the losses in the plasma prevent the appearance of pairs of improper complex conjugate modes.

IV. Conclusion

In this paper, the authors have presented a simple and systematic technique for studying general multilayered chiral waveguides based on the transition matrix approach. The method of analysis is mainly numerical and reduces the determination of the modal propagation constants for the chiral waveguide to the computation of the zeros of the determinant of a 2×2 matrix. One of the advantages of the presented scheme is that the number of layers in the waveguide, and its possible complexity hardly affects its whole performance and efficiency. Despite the method being basically numerical, the values and main features of the electromagnetic field are readily determined.

The examples considered have been focussed on the analysis of waveguides with chiral (biiso/bianisotropic) materials. In this way, the results obtained using the present method have been checked with those reported by others authors for biisotropic closed and open waveguides, showing a total agreement. All the examples of open chiral waveguides have been completed, including the dispersion of the improper modes. For the analyzed ranges of the chirality parameters, it has been found that the proper and improper modes behave in a similar way to that exhibited in the nonchiral case, although the chirality would provide another parameter to control the propagation characteristics. The authors have also studied the effects of substrate losses in the dispersion relation of a chiral waveguides, equally finding that these effects are similar to the nonchiral cases. The study of the fundamental mode of a biisotropic waveguide, when increasing either the dielectric permittivity or the chiral parameter, has showed that chiral materials could be used as an alternative to high permittivity substrates.

Finally, the authors have considered the analysis of a complex three-layer open waveguide. As in the previous examples, the behavior of the proper and improper modes have been considered and was found to be qualitatively similar to that corresponding to nonchiral cases.

REFERENCES

[1] D. L. Jaggard, A. R. Mickelson, and C. H. Papas, "On electromagnetic waves in chiral media," *Appl. Phys.*, vol. 18, pp. 211–216, 1979.

[2] K. W. Whites, "Full-wave computation of constitutive parameters for lossless composite chiral materials," *IEEE Trans. Antennas Propagat.*, vol. 43, pp. 376–384, Apr. 1995.

[3] H. Cory, "Chiral devices—An overview of canonical problems," *J. Electro. Waves Applicat.*, vol. 9, pp. 805–829, 1995.

[4] A. H. Sihvola and I. V. Lindell, "Biisotropic constitutive relations," *Microwave Opt. Technol. Lett.*, vol. 4, pp. 295–297, 1991.

[5] A. H. Sihvola, "Are nonreciprocal biisotropic media forbidden indeed?," *IEEE Trans. Microwave Theory Tech.*, vol. 43, pp. 2160–2162, Sept. 1995.

[6] J. C. Monzon, "Radiation and scattering in homogeneous general biisotropic regions," *IEEE Trans. Antennas Propagat.*, vol. 38, pp. 227–235, Feb. 1990.

[7] R. D. Graglia, P. L. E. Uslenghi, and R. E. Zich, "Dispersion relation for bianisotropic materials and its symmetry properties," *IEEE Trans. Antennas Propagat.*, vol. 39, pp. 83–90, Jan. 1991.

[8] N. Engheta, D. L. Jaggard, and M. W. Kowarz, "Electromagnetic waves in faraday chiral media," *IEEE Trans. Antennas Propagat.*, vol. 40, pp. 367–373, Apr. 1992.

[9] A. Lakhtakia and W. S. Weiglhofer, "Axial propagation in general helicoidal bianisotropic media," *Microwave Opt. Technol. Lett.*, vol. 6, pp. 804–806, Nov. 1993.

[10] C. M. Krowne, "Electromagnetic properties of nonreciprocal composite chiral-ferrite media," *IEEE Trans. Antennas Propagat.*, vol. 9, pp. 1289–1295, Sept. 1993.

[11] I. V. Lindell and F. Olyslager, "Duality transformations, green dyadics and plane-wave solutions for a class of bianisotropic media," *J. Electro. Waves Applicat.*, vol. 9, pp. 85–96, 1995.

[12] P. Pelet and N. Engheta, "The theory of chirowaveguides," *IEEE Trans. Antennas Propagat.*, vol. 38, pp. 90–98, Jan. 1990.

[13] N. Engheta and P. Pelet, "Mode orthogonality in chirowaveguides," *IEEE Trans. Microwave Theory Tech.*, vol. 38, pp. 1631–1634, Nov. 1990.

[14] H. Cory, "Wave propagation along a closed rectangular chirowaveguide," *Microwave Opt. Technol. Lett.*, vol. 6, pp. 797–800, Nov. 1993.

[15] L. Zhang, Y. Jiao, and C. Liang, "The dominant mode in a parallel-plate chirowaveguide," *IEEE Trans. Microwave Theory Tech.*, vol. 42, pp. 2009–2012, Oct. 1994.

[16] A. Toscano and L. Vegni, "Effects of chirality admittance on the propagating modes in a parallel-plate waveguide partially filled with a chiral slab," *Microwave Opt. Technol. Lett.*, vol. 6, pp. 806–809, Nov. 1993.

[17] F. Mariotte and N. Engheta, "Reflection and transmission of guided electromagnetic waves at an air-chiral interface and at a chiral slab in a parallel-plate waveguide," *IEEE Trans. Microwave Theory Tech.*, vol. 11, pp. 1895–1906, Nov. 1993.

[18] C. R. Paiva and A. M. Barbosa, "A method for the analysis of biisotropic planar waveguides—Application to a grounded chiroslabguide," *Electromagnetics*, vol. 11, pp. 209–221, 1991.

[19] I. V. Lindell, "Variational method for the analysis of lossless bi-isotropic (nonreciprocal chiral) waveguides," *IEEE Trans. Microwave Theory Tech.*, vol. 40, pp. 402–405, Feb. 1992.

[20] Z. Shen, "The theory of chiroferrite waveguides," *Microwave Opt. Technol. Lett.*, vol. 6, pp. 397–401, June 1993.

[21] Y. Wenyan and L. Pao, "The analysis of propagation characteristics in planar gyrotropic chirowaveguides," *Microwave Opt. Technol. Lett.*, vol. 6, pp. 684–689, Sept. 1993.

[22] Y. Wenyan, W. Wenbing, and L. Pao, "Guided electromagnetic waves in gyrotropic chirowaveguides," *IEEE Trans. Microwave Theory Tech.*, vol. 42, pp. 2156–2163, Nov. 1994.

[23] M. S. Kluskens and E. H. Newman, "A microstrip line on a chiral substrate," *IEEE Trans. Microwave Theory Tech.*, vol. 39, pp. 1889–1891, Nov. 1991.

[24] F. Mesa and M. Horno, "Computation of proper and improper modes in multilayered bianistropic waveguides," *IEEE Trans. Microwave Theory Tech.*, vol. 43, pp. 233–235, Jan. 1995.

[25] L. B. Felsen and N. Marcuvitz. *Radiation and Scattering of Waves*. Englewood Cliffs, NJ: Prentice-Hall, 1973.

[26] C. M. Krowne, "Fourier transformed matrix method of finding propagation characteristics of complex anistropic layered media," *IEEE Trans. Microwave Theory Tech.*, vol. 32, pp. 1617–1625, Dec. 1984.

[27] J. L. Tsalamengas, "Interaction of electromagnetic waves with general bianisotropic slabs," *IEEE Trans. Microwave Theory Tech.*, vol. 40, pp. 1870–1878, Oct 1992.

[28] R. D. Graglia, P. L. E. Uslenghi, and R. E. Zich, "Reflection and transmission for planar structures of bianistropic media," *Electromagnetics*, vol. 11, pp. 193–208, 1991.

[29] A. Ishimaru, *Electromagnetic Wave Propagation, Radiation and Scattering*, Englewood Cliffs, NJ: Prentice-Hall, 1991.

[30] C. G. Hsu, R. F. Harrington, J. R. Mautz, and T. P. Sarkar, "On the location of leaky waves poles for a grounded dielectric slab," *IEEE Trans. Microwave Theory Tech.*, vol. 39, pp. 346–349, Feb. 1991.

Gonzalo Plaza was born in Cádiz, Spain, on November, 26th, 1960. He received the *Licenciado* and the *Doctor* degrees in physics from the University of Seville, Seville, Spain, in 1986 and 1995, respectively.

He is currently an Assistant Professor in the Department of Applied Physics at the University of Seville. His research interest focuses on electromagnetic propagation in planar lines with general bianisotropic materials.

Francisco Mesa was born in Cádiz, Spain, on April 15th, 1965. He received the *Licenciado* and the *Doctor* degrees, both in physics, from the University of Seville, Spain, in 1989 and 1991, respectively.

He is currently an Associate Professor in the Department of Applied Physics at the University of Seville. His research interest focuses on electromagnetic propagation/radiation in planar lines with general anisotropic materials.

Manuel Horno (M'75) was born in Torre del Campo, Jaén, Spain. He received the *Licenciado* and the *Doctor* degrees, both in physics, from the University of Seville, Seville, Spain, in 1969 and 1972, respectively

Since October 1969 he has been with the Department of Electronic and Electromagnetism, the University of Seville, where he became as an Assistant Professor, Associate Professor, and Professor, in 1970, 1975, and 1986, respectively. His main fields of interest include boundary value problems in electromagnetic theory, wave propagation through anisotropic media, and microwave integrated circuits. He is presently engaged in the analysis of planar transmission lines embedded in anisotropic materials, multiconductor transmission lines, and planar slow-wave structures. He is a member of the Electromagnetism Academy of the Massachusetts Institute of Technology (MIT), Cambridge, MA.